International Journal of Heat and Fluid Flow 30 (2009) 715–728

Contents lists available at ScienceDirect

International Journal of Heat and Fluid Flow

journal homepage: www.elsevier.com/locate/ijhff

Prediction of amount of entrained droplets in vertical annular two-phase flow

Pravin Sawant [a,*], Mamoru Ishii [a], Michitsugu Mori [b,1]

[a] Purdue University, School of Nuclear Engineering, 400 Central Dr., West Lafayette, IN 47907-2017, USA
[b] Tokyo Electric Power Co. Inc., 4-1 Egasaki-cho, Tsurumi-ku, Yokohama 230-8510, Japan

ARTICLE INFO

Article history:
Received 29 May 2008
Accepted 6 March 2009
Available online 23 April 2009

Keywords:
Two-phase flow
Annular flow
Entrainment fraction
Droplet entrainment rate
Droplet deposition rate
Maximum entrainment fraction
Dryout

ABSTRACT

Prediction of amount of entrained droplets or entrainment fraction in annular two-phase flow is essential for the estimation of dryout condition and analysis of post dryout heat transfer in light water nuclear reactors and steam boilers. In this study, air–water and organic fluid (Freon-113) annular flow entrainment experiments have been carried out in 9.4 and 10.2 mm diameter test sections, respectively. Both the experiments covered three distinct pressure conditions and wide range of liquid and gas flow conditions. The organic fluid experiments simulated high pressure steam–water annular flow conditions. In each experiment, measurements of entrainment fraction, droplet entrainment rate and droplet deposition rate have been performed by using the liquid film extraction method. A simple, explicit and non-dimensional correlation developed by Sawant [Sawant, P.H., Ishii, M., Mori, M., 2008. Droplet entrainment correlation in vertical upward co-current annular two-phase flow. Nucl. Eng. Des. 238 (6), 1342–1352] for the prediction of entrainment fraction is further improved in this study in order to account for the existence of critical gas and liquid flow rates below which no entrainment is possible.

Additionally, a new correlation is proposed for the estimation of minimum liquid film flow rate at the maximum entrainment fraction condition. The improved correlation successfully predicted the newly collected air–water and Freon-113 entrainment fraction data. Furthermore, the correlations satisfactorily compared with the air–water, helium–water and air–genklene experimental data measured by Willetts [Willetts, I.P., 1987. Non-aqueous annular two-phase flow. D.Phil. Thesis, University of Oxford]. However, comparison of the correlations with the steam–water data available in literature showed significant discrepancies. It is proposed that these discrepancies might have been caused due to the inadequacy of the liquid film extraction method used to measure the entrainment fraction or due to the change in mechanism of entrainment under high liquid flow conditions.

1. Introduction

Annular two-phase flow is one of the most important two-phase flow regimes encountered in operation of several industrial equipments such as steam boilers, refrigeration systems, nuclear reactors and many other gas–liquid contacting types of equipments in chemical industry. It occurs at relatively high gas velocity conditions at which the part of liquid flow in the form of a liquid film adjacent to the wall and remaining liquid flow in the form of droplets entrained in the central gas core flow. One of the advantages of having this flow regime in heat transfer applications such as steam boilers and boiling water nuclear reactors is that it offers very high convective heat transfer coefficient due to presence thin liquid film. However, the heat transfer can severely deteriorate if the liquid film dries out after its continuous thinning due to the combined effect of entrainment of droplets from the liquid film, deposition of droplets on to the liquid film and evaporation. Therefore, accurate prediction of amount of entrained droplets or entrainment fraction in annular flow is essential for the estimation of dryout condition and for the analysis of post-dryout heat transfer. Furthermore, design correlations for the prediction of pressure drop and mass transfer in annular flow also depends on the estimation of amount of entrained droplets.

Vertical annular two-phase flow itself can be classified into several flow regimes. Fig. 1 shows the flow regime map plotted for the air–water flow in 9.4 mm diameter tube at 1.2 bar. It is obtained from the flow regime transition criteria proposed by Mishima and Ishii (1984). The figure also shows an onset of entrainment (OE) boundary (dashed line) derived from Ishii and Grolmes's (1975) onset of entrainment criterion. The OE boundary divides annular flow regime into two sub-regimes; annular flow with entrained droplets and annular flow without entrained droplets. Also it can be observed that the OE boundary shows two limiting conditions, a critical gas velocity ($\langle j_g \rangle_{cr}$) below which no entrainment is possible at any liquid flow rate and a critical liquid velocity ($\langle j_f \rangle_{cr}$)

* Corresponding author. Tel.: +1 7654963571; fax: +1 765 494 9570.
E-mail addresses: psawant@purdue.edu (P. Sawant), ishii@purdue.edu (M. Ishii), michitsugu.mori@tepco.co.jp (M. Mori).
[1] Tel.: +81 45 613 6704; fax: +81 45 613 7899.

0142-727X/$ - see front matter © 2009 Elsevier Inc. All rights reserved.
doi:10.1016/j.ijheatfluidflow.2009.03.003

Nomenclature

a	Reynolds number dependent parameter, Eq. (3) [–]
D	diameter [m]
E	entrainment fraction [–]
g	gravitational acceleration [m s^{-2}]
$\langle j_f \rangle$	area averaged superficial liquid velocity [m s^{-1}]
$\langle j_g \rangle$	area averaged superficial gas velocity [m s^{-1}]
$N_{\mu f}$	viscosity number, Eq. (12) [–]
p	pressure [N m^{-2}]
On	Onhenzoge number, Eq. (17) [–]
Re	Reynolds number, Eq. (6) [–]
T	temperature [K]
We	Weber number, Eq. (5) [–]

Greek symbols

μ	dynamic viscosity [kg m^{-1} s^{-1}]
ρ	mass density [kg m^{-3}]
σ	surface tension [N m^{-1}]

Subscripts

32	Sauter mean diameter
cr	critical
g	gas phase
f	liquid phase
ff	liquid film
max	maximum
min	minimum
vm	volume mean diameter

Abbreviations

DW	disturbance waves
RW	ripple waves
ODW	onset of disturbance waves
OE	onset of entrainment

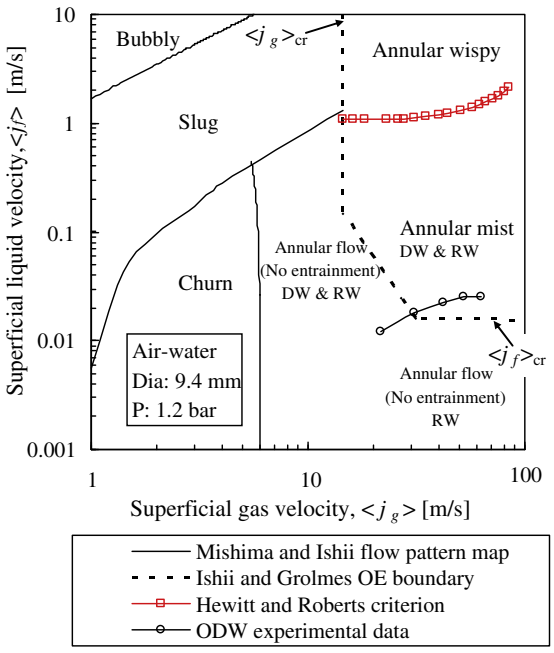

Fig. 1. Annular two-phase flow regimes.

below which no entrainment is possible at any gas velocity. In a transition region between these two limiting conditions, the critical gas velocity at the onset of entrainment increases with the decrease in liquid velocity. Ishii and Grolmes (1975) developed this criterion based on a mechanism of shearing off the crest of disturbance waves. They assumed that the onset of entrainment takes place when the drag force on the tip of disturbance waves exceeds the retaining force of surface tension. Also it can be observed that the gas velocity required for the onset of entrainment increases very sharply at the critical liquid velocity, $\langle j_f \rangle_{cr}$. Based on the experimental data on onset of entrainment, Ishii and Grolmes proposed that this critical liquid velocity is correspond to the liquid film Reynolds number (Re_{ffOE}) 160. They also proposed that for $Re_{ffOE} < 160$, suppression of entrainment takes place due to the suppression of disturbance waves.

Interfacial waves traversing the liquid film surface in annular flow are mainly classified into two categories, the disturbance waves (DW) and ripple waves (RW) (Asali, 1984; Sawant et al., 2008b). A liquid film interface in the annular flow with entrained droplets is covered by the both type of waves, however, the annular flow without entrainment is further divided into two regimes by an onset of disturbance wave (ODW) boundary. Although the ODW boundary is not well established and no analytical or empirical criterion is available for its prediction, the experimental data have showed that for liquid flow rates below the ODW boundary, the liquid film surface is covered only by ripple waves (Asali, 1984; Azzopardi, 1997; Hills, 1997). Furthermore, it has been also observed from the experimental data that initially at low gas velocity, a liquid velocity at the ODW increases with the increasing gas velocity and eventually under high gas velocity condition it asymptotically approaches a constant value similar to the critical liquid velocity at the onset of entrainment (see Section 4 for further detailed discussion and experimental data on ODW). As mentioned earlier, Ishii and Grolmes (1975) proposed that this asymptotic critical liquid velocity is correspond to the liquid film Reynolds number160. In Fig. 1, the experimental data on ODW obtained in the current study is also plotted. Although the current data shows that the asymptotic liquid velocity or the critical liquid velocity at ODW is higher than the prediction of Ishii and Grolmes criterion, considering an empirical nature of the criterion and significant errors in measurement of OE (Ishii and Grolmes, 1975), the two conditions can be assumed similar. However, at lower gas velocity, the trends shown by ODW and OE conditions are opposite. The ODW boundary shows that the liquid velocity at ODW decreases with the decreasing gas velocity and the OE boundary shows the liquid velocity at the OE increases with the decreasing gas velocity. Thus it appears that only under high gas velocity, the conditions for OE and ODW are similar. This conclusion is in contrast to the assumption of several previous researchers (Azzopardi, 1997; Hills, 1997) that the OE and ODW conditions are always similar. It can be also concluded that the presence of disturbance waves on the liquid film surface is necessary but not sufficient condition for OE.

In the annular with entrained droplets, as liquid velocity is increased for a given gas velocity, a flow regime transition from annular mist to annular wispy flow is observed (Hawkes et al., 2000). An empirical transition criteria proposed by Hewitt and Roberts (1969) for the prediction of this transition is shown in Fig. 1. The experimental observations have shown the existence of wisps or agglomerated liquid structure in a gas core of wispy annular flow (Bennett et al., 1965). However, surprisingly very limited information is available on the nature of interfacial waves in

annular wispy flow regime as well as in a transition regime between the annular mist and annular wispy flow. Sekoguchi and Takeishi (1989) reported the existence of huge waves in these regimes which they described as larger and faster waves compared to the regular disturbance waves. It is expected that in annular wispy flow and in the transition regimes, mechanism of entrainment can be quite different. Furthermore, in these flow regimes, measurement of liquid film flow rate using the liquid film extraction method used in the current study and in most other annular flow studies is very difficult due to the possibility of incomplete extraction. Therefore, the current experimental data and newly developed correlation for entrainment fraction are limited to annular mist flow regime only. More detailed studies of the transition from annular mist to annular wispy flow regime and interfacial wave characteristics in these flow regimes are the part of future work. Also, it should be noted that several of the existing experimental data on measurement of entrainment fraction in steam–water system analyzed in Section 5 of this paper are obtained at very high liquid phase Reynolds number conditions which may correspond to the transition regime or annular wispy flow regime.

In what follows, a simple and explicit correlation is developed for the prediction of entrainment fraction in annular flow and compared with the extensive amount of experimental data obtained in the current study as well as the data available in literature. A summary of previously developed correlation by Sawant et al. (2008a) for the prediction of entrainment fraction is presented in Section 2 along with the discussion on its shortcomings. In Section 4, improved correlation approach is presented in order to overcome these shortcomings. Experimental test facilities used to perform air–water and Freon-113 annular flow experiments are presented in Section 3. Finally, in Section 5, the newly developed correlation is compared with the experimental data.

2. Previous work

Simple, explicit and non-dimensional entrainment fraction correlation applicable over wide range of flow and pressure conditions is necessary for the implementation in various nuclear reactor thermal hydraulic system analysis codes such as RELAP5 (Reactor Excursion and Leak Analysis Program) and TRACE (TRAC RELAP Advanced Computational Engine). Towards this end, Sawant et al. (2008a) developed a correlation for the prediction of entrainment fraction based on their annular flow air–water experimental data obtained in 9.4 mm diameter test section at three different pressure conditions. Their experimental data as plotted in Fig. 2 shows that for a given liquid flow rate, as gas velocity increases, entrainment fraction also increases and eventually under very high gas velocity it asymptotically approaches a limiting condition of maximum entrainment fraction (E_{max}) or minimum liquid film flow rate. Further increase of gas velocity does not affect entrainment fraction or liquid film flow rate. Furthermore, this minimum liquid film flow rate at the maximum entrainment fraction condition is found to be always larger than the critical liquid film flow rate at the onset of entrainment or onset of disturbance wave under high gas velocity condition for which Ishii and Grolmes (1975) proposed liquid film Reynolds number 160. The experimental data also shows that the maximum entrainment fraction as well as the minimum liquid film flow rate increases with the increase in total liquid phase Reynolds number (also see Fig. 5). Sawant et al. (2008a) compared the data with the existing entrainment fraction correlations and found that the correlations either failed to predict the maximum entrainment fraction trends under high gas velocity or the effect of pressure (or density ratio change) on entrainment fraction. However, since the experimental data was completely described by the two non-dimensional numbers, Weber number (Eq. (5)) and liquid phase Reynolds number (Eq. (6)), a new correlation was proposed by Sawant et al. (2008a) to predict the entrainment fraction based on these non-dimensional numbers as given below;

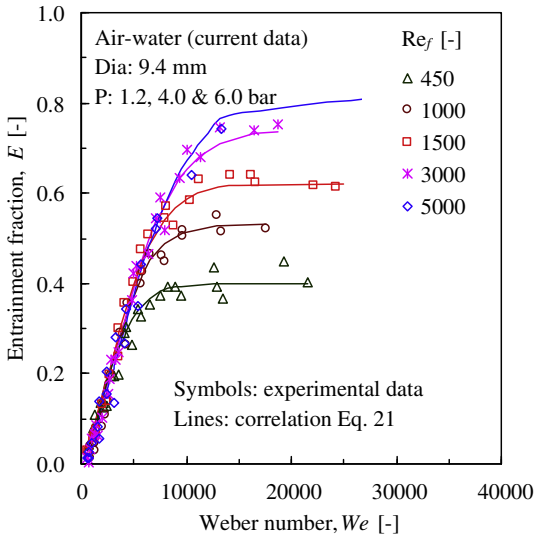

Fig. 2. Air–water entrainment fraction data.

$$E = E_{\max}\tanh(aWe^{1.25}) \tag{1}$$

where, E, E_{max} and a are entrainment fraction, maximum entrainment fraction and liquid phase Reynolds number dependent parameter, respectively. E_{max} and a are defined as follows;

$$E_{\max} = 1 - \frac{Re_{ff\,\min}}{Re_f} \tag{2}$$

$$a = 2.31\times 10^{-4} Re_f^{-0.35} \tag{3}$$

where, Re_f and Re_{ffmin} are total liquid phase Reynolds number and minimum liquid film Reynolds number at the condition of maximum entrainment fraction, respectively. Empirical equation developed based on the air–water data was proposed for the prediction of Re_{ffmin} as given below;

$$Re_{ff\,\min} = 250\ln(Re_f) - 1265 \tag{4}$$

Weber number and liquid phase Reynolds number are defined as follow;

$$We = \frac{\rho_g \langle j_g\rangle^2 D}{\sigma}\left(\frac{\Delta\rho}{\rho_g}\right)^{1/4} \tag{5}$$

$$Re_f = \frac{\rho_f \langle j_f\rangle D}{\mu_f} \tag{6}$$

where, D, $\langle j_f\rangle$, $\langle j_g\rangle$, ρ_f, ρ_g, σ, μ_f and μ_g are test section diameter, area average superficial liquid velocities, area average superficial gas velocity, liquid phase density, gas phase density, surface tension, liquid phase viscosity and gas phase viscosity, respectively. It was proposed that the dependence of parameters a and Re_{ffmin} on liquid phase Reynolds number (Re_f) is due to the effect of entrained droplets on gas phase turbulence.

The above correlation has been satisfactorily compared with several air–water entrainment fraction data. However, the dependence of parameter a and Re_{ffmin} on fluid properties is not known. Furthermore, the correlation, Eq. (1) do not account for the existence of critical gas velocity as well as critical liquid flow rate below which no entrainment is possible. The correlation for Re_{ffmin}, Eq. (4) is purely empirical and shows that Re_{ffmin} approaches zero as Re_f approaches zero. Instead Re_{ffmin} should approach the liquid

film Reynolds number at the onset of entrainment, Re_{ffOE} as Re_f approaches Re_{ffOE}.

In view of the above discussion, in the following study, improved correlations are proposed for entrainment fraction (E) and Re_{ffmin}. The new correlation for entrainment fraction is compared with the air–water and Freon-113 entrainment fraction data obtained in this study as well as air–water, helium-water, air-genklene and steam–water data available in literature.

3. Experiment

Two types of experiments have been carried out; air–water experiments and organic fluid experiments. The air–water experiments have been performed in 9.4 mm diameter test section at three pressure conditions; 1.2, 4.0 and 6.0 bar. The organic fluid experiments also covered three pressure conditions; 2.8, 5.0 and 8.5 bar. The diameter of test section in organic fluid experiments was 10.2 mm. In both the experiments, measurements of entrainment fraction, droplet entrainment rate and droplet deposition rate have been performed in an equilibrium annular flow by using the liquid film extraction method (Sawant et al., 2007, 2008b). Additionally, double ring type conductance probes have been used to measure the liquid film thickness, ODW conditions and disturbance wave properties in the air–water experiments (Sawant et al., 2008b).

Detailed information about the design and operation of the air–water test facility, liquid film extraction method and parametric range covered in the air–water experiments is available in Sawant et al. (2007, 2008a). The experimental data on entrainment fraction measurements in air–water experiments have been analyzed in Sawant et al. (2008a) for the development of entrainment fraction correlation Eq. (1). Sawant et al. (2008b) presented the analysis of liquid film thickness and disturbance wave property measurement data. In this study, the air–water entrainment fraction data and ODW wave data are utilized for the development of improved correlations for entrainment fraction and Re_{ffmin}.

A simplified schematic drawing of the experimental test facility used to perform the organic fluid experiments is shown in Fig. 3. The organic fluid experiments have been carried with Freon-113 liquid and gas phases under thermal equilibrium conditions. Due to its low critical pressure, Freon-113 can simulate high pressure conditions representative of steam–water flow in nuclear reactors at relatively low pressure. The test facility can be divided into four major parts; vapor supply system (not shown in Fig. 3), liquid supply system, pressurizer system (not shown in Fig. 3) and test section. The vapor supply system consists of an evaporator having 20 kW heating capacity and 0.18 m^3 volume used for the generation of Freon-113 vapor phase, ventury flow meter for the vapor mass flow rate measurement and control valve for the adjustment of vapor flow rate. The evaporator is dynamically decoupled from the test section to prevent the instabilities. The liquid supply system consists of centrifugal pump, turbine flow meter, pre-heater, condenser and storage tank. The multistage high pressure centrifugal pump circulates liquid Freon-113 through the bypass loop, pre-heater, test section and condenser. The liquid flow rate is measured using Sponsler turbine flow meter, model MF20-90. An immersion heater having 5 kW capacity is used to preheat the liquid phase up to the saturation temperature. A tape heater (760 W), wrapped around the inlet liquid line is also used to preheat the inlet liquid phase. Freon-113 vapor and liquid phase mixture exits from the top of test section and mixes with the cold

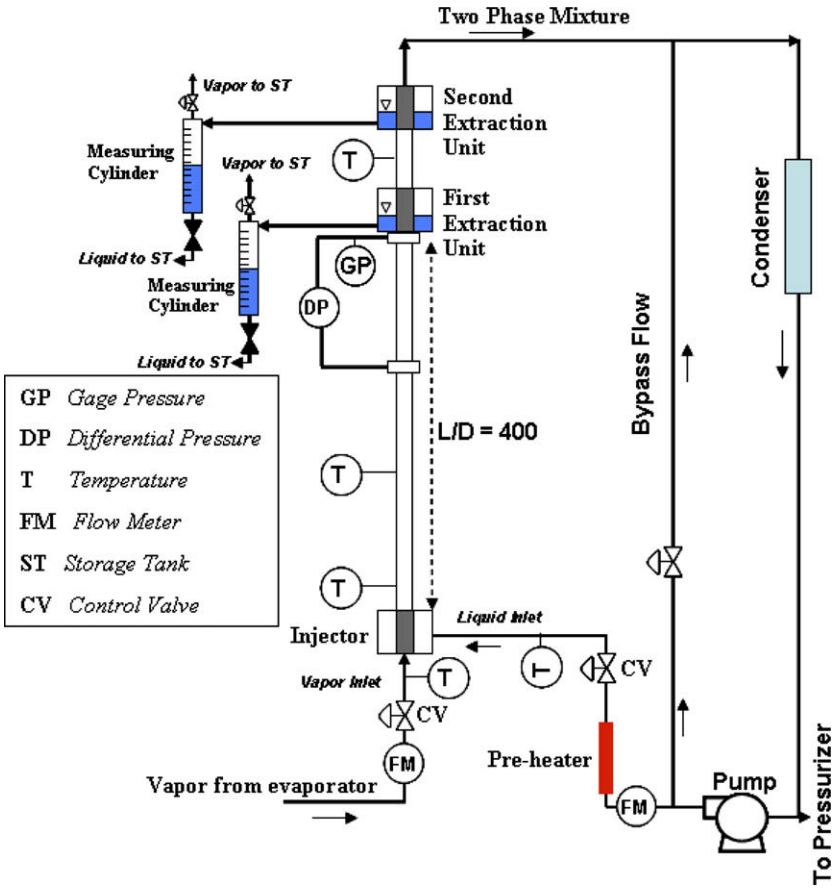

Fig. 3. Schematic of Freon-113 test facility.

bypass liquid flow. The mixture is then further cooled in a plate type of condenser with cold water on the secondary side. A stainless steel storage tank having capacity of 0.3 m^3 is used to collect the liquid film extracted in the extraction units. The test section pressure is maintained using the pressurizer system which consist of pressurizer tank, nitrogen buffer tank and high pressure nitrogen cylinder. Major components of the test section are injector unit and two extraction units with measuring cylinders. Designs of the mixture unit, first extraction unit, second extraction unit and measuring cylinder are essentially similar to the designs of these components in the air–water test facility (Sawant et al., 2007, 2008a). However, operation of extraction units in the organic fluid experiments required extra care due to the condensation of vapor phase. The test section and extraction units are carefully insulated to keep the experiments as close to adiabatic condition as possible. Pressure taps are provided on the test section for the measurement of pressure drop and system pressure.

The injector unit and extraction units consist of a central porous tube with 100 μm porosity. In the injector, liquid phase is injected into the test section through the wall of this porous tube while in the extraction units, liquid film is extracted through the wall of porous tube by creating a small pressure difference across the wall. The extracted liquid film flow rate is measured using the measuring cylinders. After the injector unit, a developing length of 400D is provided before performing any measurements. This insured that all the measurements are obtained in fully developed annular flow. Entrainment fraction is derived from the liquid film flow rate measured at first extraction unit and total liquid flow rate at inlet while entrainment and deposition rates are obtained from the liquid film flow rate measured at second extraction unit. A deposition length between the two extraction units is 45 cm.

Table 1 shows the range of flow rates covered at each pressure condition in Freon-113 experiments. Fig. 4 shows the experimental conditions plotted on Mishima and Ishii (1984) flow regime map.

Table 1
Range of experimental parameters in Freon-113 experiments.

P [bar]	$\langle j_f \rangle$ [m/s]	$\langle j_g \rangle$ [m/s]
2.8	0.08–0.40	12–24
5.0	0.13–0.40	11–17
8.5	0.13–0.40	6–11

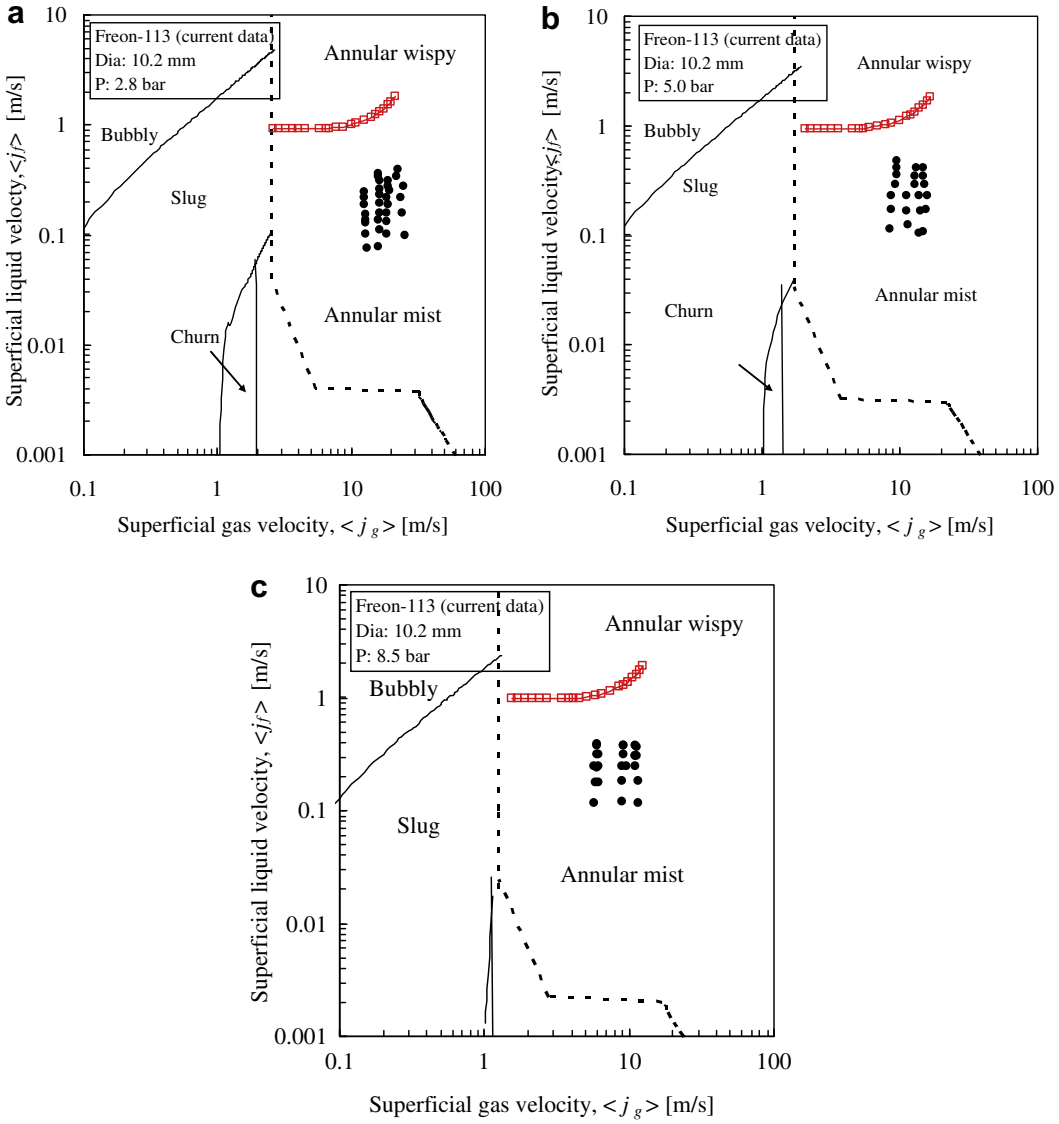

Fig. 4. Flow conditions in Freon-113 experiments: (a) P: 2.8 bar, (b) P: 5.0 bar and (c) P: 8.5 bar.

Similar experiments have been performed by Lopez de Bertodano et al. (2001), however, their experiments covered very small range of flow conditions compared to the current data.

4. Correlation approach

As discussed in Section 2, the previously developed entrainment fraction correlation in Eq. (1) should be improved in order to account for the existence of critical gas velocity and critical liquid flow rate at the onset of entrainment. Also the improved correlation is necessary for $Re_{ff\min}$. The following modified correlation is considered in order to address these issues;

$$E = E_{\max}\tanh[a(We - We_{cr})^{1.25}] \tag{7}$$

$$E_{\max} = 1 - \frac{Re_{ff\,\min}}{Re_f} = 1 - \frac{Re_{ffOE} + f(Re_f - Re_{ffOE})}{Re_f} \tag{8}$$

where, We_{cr} and Re_{ffOE} are critical Weber number corresponds to the critical gas velocity at the onset of entrainment and liquid film Reynolds number at the onset of entrainment under high gas velocity condition, respectively. The above correlation indicates that as gas velocity approaches the critical gas velocity, Weber number approaches the critical Weber number and entrainment fraction approaches zero. Similarly, the correlation for $Re_{ff\min}$ accounts for the existence of critical liquid flow rate at the onset of entrainment under high gas velocity;

$$Re_{ff\,\min} = Re_{ffOE} + f(Re_f - Re_{ffOE}) = Re_{ffOE} + f(Re_{fEX}) \tag{9}$$

where Re_{fEX} is excess liquid phase Reynolds number above Re_{ffOE}. The above correlation indicates that as the liquid phase Reynolds number, Re_f approaches Re_{ffOE}, Re_{fEX} approaches zero and $Re_{ff\min}$ approaches Re_{ffOE}. This results in E_{max} and E to approach zero. In summary:

As

$$We \to We_{cr}, \quad E \to 0.0$$

As

$$Re_f \to Re_{ffOE}, \quad Re_{fEX} \to 0.0 \quad \text{and} \quad Re_{ff\,\min} \to Re_{ffOE}$$

therefore,

$$E_{\max} \to 0.0 \quad \text{and} \quad E \to 0.0$$

While the above approach shows the correct trends at the limiting conditions of critical gas velocity and critical liquid flow rate, the correlations are necessary for We_{cr}, Re_{ffOE} and $f(Re_{fEX})$. A correlation for critical Weber number, We_{cr} is discussed in Section 4.1. Function $f(Re_{fEX})$ accounts for the effect of entrained droplets on $Re_{ff\min}$. The experimental data have shown that $Re_{ff\min}$ is always greater than Re_{ffOE} (Sawant et al., 2008a) and it increases as the total liquid phase Reynolds number increases. In Fig. 5, $Re_{ff\min}$ measured in air–water experiments is plotted against the liquid phase Reynolds number. The data measured by Sawant et al. (2008a), Schadel (1988) and Asali (1984) are shown in the figure. As discussed in Sawant et al. (2008a), the increase of $Re_{ff\min}$ with Re_f may be due to the increase of amount droplets in the gas core flow. At the condition of onset of entrainment, gas phase is free of entrained droplets. However, as the liquid phase Reynolds number increases, the concentration of droplets in the gas core increases. It was proposed that the increased droplet concentration may cause the suppression of gas phase turbulence leading to the decreased interaction between the gas core flow and liquid film. In order to develop a correlation for the $Re_{ff\min}$ it is necessary to model Re_{ffOE} and effect of Re_{fEX}. Additionally, the dependence of these parameters on fluid properties should be analyzed. Further analysis for the development of correlation for $Re_{ff\min}$ is presented in Section 4.2.

4.1. Critical gas velocity at the onset of entrainment

Several correlations have been developed for the prediction of critical gas velocity at the onset of entrainment (Ishii and Grolmes, 1975; Azzopardi, 1997). Ishii and Grolmes compared the existing dimensional and non-dimensional correlations with the experimental data and found significant discrepancies among the predictions of different correlations. They concluded that the correlations lacked the physical understanding of onset of entrainment phenomenon. Following very rigorous analysis of the mechanisms of entrainment they proposed a comprehensive correlation for the prediction of critical gas velocity at the onset of entrainment. Here the correlation proposed for low viscosity liquids such as water having viscosity number, $N_\mu < 1/15$ is presented;

For $Re_{ff} > 1635$;

$$\frac{\mu_f \langle j_g \rangle_{cr}}{\sigma}\sqrt{\frac{\rho_g}{\rho_f}} \geqslant N_\mu^{0.8} \tag{10}$$

For $1635 > Re_{ff} > 160$

$$\frac{\mu_f \langle j_g \rangle_{cr}}{\sigma}\sqrt{\frac{\rho_g}{\rho_f}} \geqslant 11.78 N_\mu^{0.8} Re_{ff}^{-1/3} \tag{11}$$

where,

$$N_\mu = \frac{\mu_f}{\left(\rho_f \sigma \sqrt{\frac{\sigma}{g\Delta\rho}}\right)^{1/2}} \tag{12}$$

It can be seen from Eq. (10) that the critical gas velocity for $Re_{ff} > 1635$ is independent of liquid film flow rate. Ishii and Grolmes defined this regime as a rough turbulent regime in which interfacial transfer of momentum is independent of liquid film flow rate. For the transition regime defined for $1635 > Re_{ff} > 160$, the critical gas velocity is function of liquid film Reynolds number. As mentioned earlier, for $Re_{ff} < 160$, Ishii and Grolmes proposed that the critical gas velocity required for the onset of entrainment increases very significantly and limiting condition of critical liquid flow rate at the onset of entrainment is reached. A correlation for this critical liquid film flow rate is presented in Section 4.2. The critical Weber number, We_{cr} can be calculated from the estimates of critical gas velocity obtained using Eqs. (10) and (11) and following correlation;

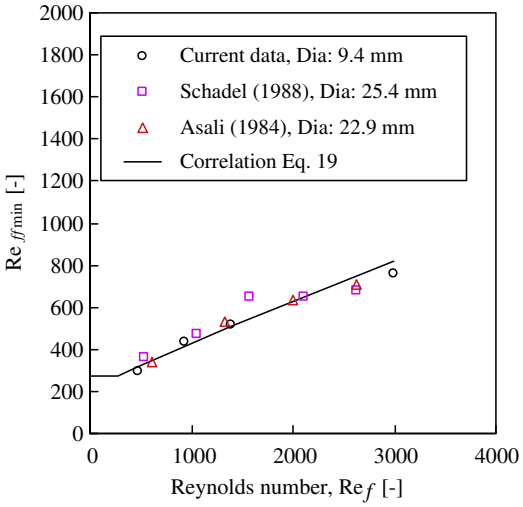

Fig. 5. Dependence of $Re_{ff\min}$ on Re_f.

$$We_{cr} = \frac{\rho_g \langle j_g \rangle_{cr}^2 D}{\sigma} \left(\frac{\Delta\rho}{\rho_g} \right)^{1/4} \quad (13)$$

More recently, Pan and Hanratty (2002) proposed an empirical correlation for the critical gas velocity based on the experimental data;

$$\frac{D^{0.5} \langle j_g \rangle_{cr} (\rho_f \rho_g)^{0.25}}{\sigma^{0.5}} \cong 40 \quad (14)$$

The above correlation can be also recast into a form similar to Ishii and Grolmes correlation;

$$\frac{\mu_f \langle j_{gcr} \rangle}{\sigma} \sqrt{\frac{\rho_g}{\rho_f}} \geqslant 40 \frac{\mu_f}{\sqrt{\sigma}} \frac{\rho_g^{1/4}}{\rho_f^{1/3}} \quad (15)$$

However, Ishii and Grolmes correlation is more rigorously developed following the physical mechanism of entrainment. Moreover, Pan and Hanratty correlation do not show the dependence of critical gas velocity on liquid film Reynolds number observed in the transition regime. Therefore, Ishii and Grolmes correlation is proposed for the calculation of critical Weber number in this study.

4.2. Correlation for minimum liquid film Reynolds number, Re_{ffmin}

Minimum liquid film Reynolds number, Re_{ffmin} is defined as the liquid film Reynolds number at the maximum entrainment fraction condition. As shown in Eq. (9), in order to estimate Re_{ffmin} it is necessary to calculate Re_{ffOE} and function $f(Re_{fEX})$ which accounts for the effect of entrained droplets on Re_{ffmin}.

4.2.1. Correlation for Re_{ffOE}

Re_{ffOE} correspond to the critical liquid film flow rate at which OE takes place under high gas velocity condition. As shown in Fig. 1, at this condition, gas velocity required for the OE increases very sharply. Ishii and Grolmes (1975), using the experimental data on OE, proposed that this condition occurs at liquid film Reynolds number 160 and if liquid flow rate falls below this Reynolds number, suppression of disturbance waves take place resulting in suppression of entrainment. However, significant discrepancies have been observed in the experimental data on OE conditions obtained using different experimental techniques (Ishii and Grolmes, 1975). In contrast to the critical gas velocity correlations in Eqs. (10) and (11) which are developed by following a rigorous analysis, the criterion, $Re_{ffOE} = 160$ is purely empirical and it may not be applicable over wide range of diameter, flow rates and fluid property conditions. In this study, a new correlation is developed for Re_{ffOE} based on the extensive database on measurement of ODW. As we have seen in Section 1, the OE and ODW occur at similar conditions under high gas velocity. In other words, under high gas velocity condition, as soon as the disturbance waves starts appearing on the surface of liquid film, OE takes place. Therefore the experimental data on ODW under high gas velocity can be used to develop a correlation for Re_{ffOE}. Furthermore, the measurement of ODW using flush mounted film thickness probe is more reliable, accurate and objective compared to the measurement of OE. Also the available experimental data on ODW covered wide range of diameter, flow and viscosity conditions (Azzopardi 1997).

Azzopardi (1997) presented a review of experimental data on measurement of ODW and OE conditions and correlations available for the prediction of these conditions. The existing experimental data on ODW is summarized in Table 2 along with the newly obtained experimental data in the current study. It can be observed that most of the experiments correspond to the atmospheric pressure condition. Only the current experimental data covered higher pressure conditions, 4.0 and 6.0 bar. The database covered a range of diameter from 9. 4 to 125 mm and a range of viscosity from 1.0 to 24.0×10^{-3} kg m^{-1}s^{-1}. The current data obtained in air–water experiments under three pressure conditions is useful to study the effect change in density ratio (ρ_f/ρ_g) on ODW. Azzopardi (1997) found that the existing correlations for ODW failed to predict the diameter and viscosity effects. They proposed the following non-dimensional relation to collapse the OE as well as ODW data;

$$Re_{ff}(On)^{0.5} \propto \frac{We}{Re_g} \quad (16)$$

where, On is Onhenzoge number.

$$On = \frac{\mu_f}{\sqrt{\sigma \rho_f D}} \quad (17)$$

$$We/Re_g = \frac{\mu_g \langle j_g \rangle}{\sigma} \quad (18)$$

However, as shown in Fig. 6, these non-dimensional numbers failed to predict the effect pressure or density ratio change observed in the current data. Contrary to this, as shown in Fig. 7, Weber number defined in Eq. (5) successfully collapsed the current data corresponding to different pressure conditions. In Fig. 7, measured liquid film Reynolds number at ODW is plotted against Weber number. In order to verify whether these non-dimensional numbers can also predict the diameter and liquid viscosity dependence, the experimental data in Table 2 is plotted in Fig. 8. The experimental data correspond to liquid viscosity, $\mu_f = 1 \times 10^{-3}$ kg m^{-1}s^{-1} are plotted in Fig. 8a to study the effect test section diameter. It can be observed the non-dimensional numbers Re_{ff} and We failed to predict the effect of diameter on ODW. The data shows that as the diameter increases, Re_{ff} at ODW decreases. Furthermore, it can be also concluded that the diameter effect is observed for the test section diameters greater than 32 mm. This may be due to the effect of diameter on the coherent nature of disturbance waves. The experimental data obtained by Martin and Azzopardi (1985) have showed that the degree of coherence of

Table 2
Onset of disturbance wave data.

Data source	Fluid system	Pressure, P [bar]	Diameter, D [mm]	Viscosity, μf [kgm^{-1} s^{-1}] $\times 10^{-3}$
Nedderman and Shearer (1963)	Air–water	1.1	32.0	1.0
Shearer and Nedderman (1965)	Air–water	1.1	32.0	1.0
Hall-Taylor et al. (1968)	Air–water	1.1	25.4	1.2–24.0
	Air-sucrose			
Azzopardi et al. (1983)	Air–water	1.1	125.0	1.0
Martin (1983)	Air–water	1.1	58.0	1.0
Asali (1984)	Air–water	1.1	42.0	1.1–4.14
	Air-glycerin			
Ohba et al. (1995)	Air–water	1.1	23.0	1.0
Current data	Air–water	1.2–6.0	9.4	1.0

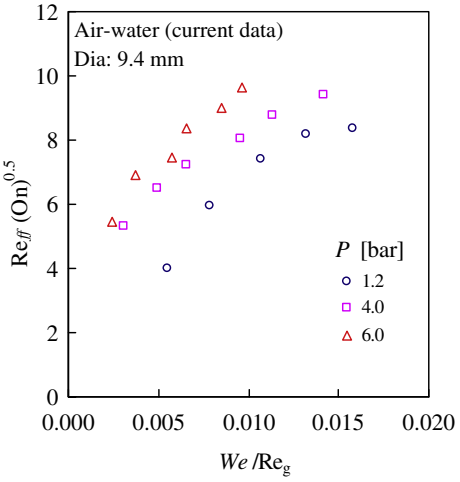

Fig. 6. Comparison of the current air–water ODW data with Azzopardi (1997) relation Eq. (16).

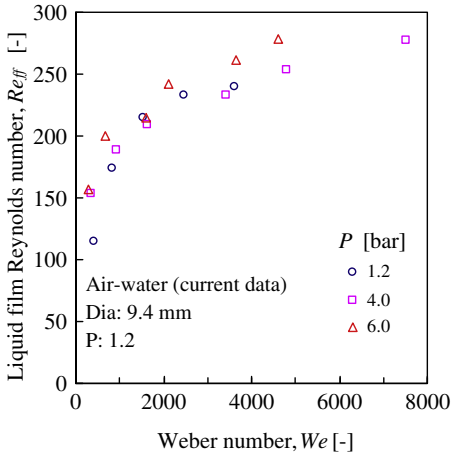

Fig. 7. Current air–water ODW data.

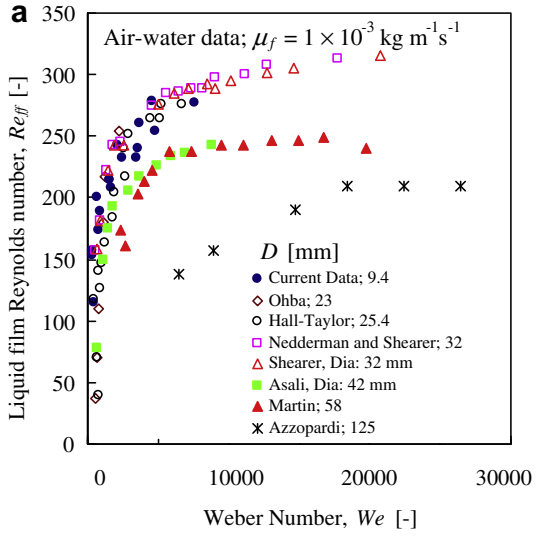

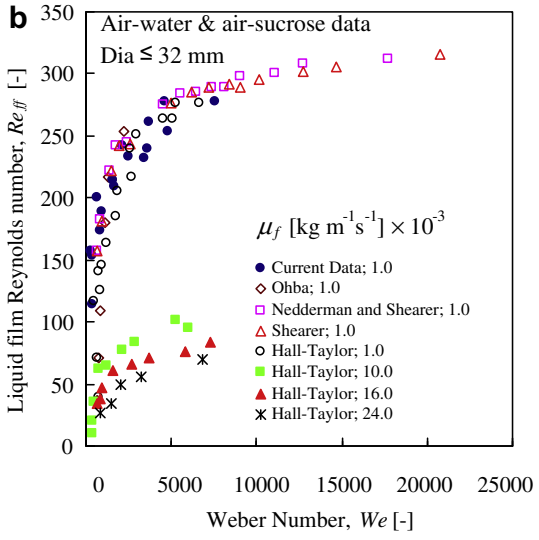

Fig. 8. ODW experimental data: (a) Effect of diameter and (b) effect of viscosity on ODW.

disturbance decreases as the diameters of test section increases. In this study, only the experimental data obtained in test section diameter up to 32 mm are used to develop a new correlation. Therefore, the new correlations for Re_{ffmin} and E are limited to the test diameters up to 32 mm. In order to study the effect of viscosity, the experimental data in small diameter test sections ($D \leqslant 32$ mm) are plotted in Fig. 8b. The data shows that as the liquid viscosity increases, Re_{ff} at ODW decreases. Viscosity number ($N_{\mu f}$) defined in Eq. (12) can be used to account for the effect of viscosity. As shown in Fig. 9, Hall-Taylor and Nedderman (1968) experimental data obtained at 1, 10, 16 and 24×10^{-3} kg m^{-1}s^{-1} viscosities can be collapsed by plotting $Re_{ff}\,(N_{\mu f})^{0.5}$ against Weber number. Hall-Taylor and Nedderman also performed experiments at $\mu_f = 5 \times 10^{-3}$ kg m^{-1}s^{-1}, however, these data showed unexpected trends and not considered in the current analysis. Finally, all the experimental data in Table 2 measured for $D \leqslant 32$ mm are plotted in Fig. 10. It can be observed that the proposed non-dimensional numbers collapsed all the data satisfactorily. Also it can be observed that under high gas velocity/Weber number, the non-dimension group, $Re_{ff}\,(N_{\mu f})^{0.5}$ asymptotically approaches a limiting value. Since in this study we are only interested in conditions of OE or ODW under high gas velocity, a correlation for Re_{ffOE} can be given as follows:

$$Re_{ffOE} = 13(N_{\mu f})^{-0.5} \tag{19}$$

While the above correlation is sufficient for the use in entrainment fraction correlation, more detailed mechanistic correlation is necessary for the prediction of ODW over all range of gas velocity.

4.2.2. Correlation for $f(Re_{fEX})$

Now we will consider the effect of entrained droplets on Re_{ffmin}. As shown in Fig. 5, Re_{ffmin} increases with the increasing liquid flow rate. Sawant et al. (2008a) proposed that this increase in Re_{ffmin} may be due to the effect entrained droplets on gas phase turbulence. They arrived at this conclusion based on Gill et al. (1964) experimental data and its analysis presented by Owen and Hewitt (1987). Gill *et al.* (1963) measured local gas phase velocities in annular flow and found that the gas velocity profile becomes more peaked as the total liquid flow rate increases for a given gas flow rate. Owen and Hewitt (1987) derived two-phase Von Karman constant (k_{tp}) by fitting the Gill's experimental data to log law equation and found that k_{tp} decreases as the concentration of droplets increases. They attributed this decrease on k_{tp} to the suppression of turbulence due to the increased droplet concentration. Similarly,

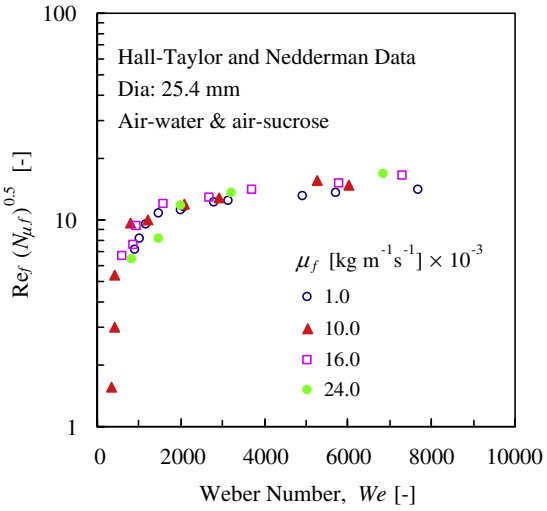

Fig. 9. Effect of viscosity on ODW.

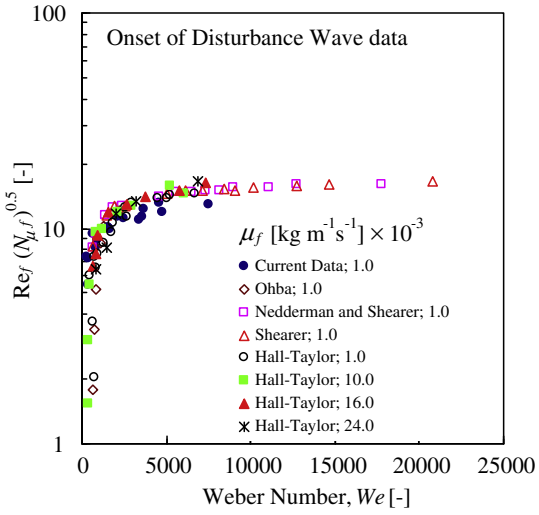

Fig. 10. A correlation for Re_{ffOE}.

Abolfadl and Wallis (1985) and Namie and Ueda (1972) also proposed that the increased droplet concentration reduces the turbulent mixing length in annular flow. However, Azzopardi (1999) found that even though the gas velocity profile is more peaked in annular flow, the measured turbulence intensity is actually higher than the corresponding gas only flow and concluded that the existence of the droplets actually enhances the turbulent intensity. They proposed that the enhancement of turbulent intensity in annular flow is due to the wavy liquid film interface and presence of newly created, slow moving droplets which are capable of shedding vortices. Additionally, Hay et al. (1996) analyzed the gas velocity profile in annular flow and showed that the peaked velocity profile is due to the increased liquid film thickness and roughness of the liquid film. In summary, there is still no consensus on the effect of entrained droplets on gas phase turbulence in annular flow.

It is expected that the effect of droplets on gas phase turbulence should depend on droplet size and velocity distribution. Consequently it is necessary to consider the variation of these parameters with gas and liquid phase flow rates. Gore and Crowe (1989), based on gas-solid particle experiments, proposed that the enhancement or suppression of turbulence depends on a ratio of particle size to turbulence length scale. If the ratio is greater than 0.1, enhancement of turbulence takes place and vice versa. Hetsroni (1989) analyzed gas-solid particle flow and deduced that the particles having particle Reynolds number (Re_p) greater than 400 increases the turbulence while the particles with Re_p less than 400 attenuate the turbulence. It was proposed that the enhancement of turbulence is due to the vortex shedding and velocity defect in the wake of particle and the attenuation is due to the work associated with the motion of particle (Azzopardi, 1999). In view of this we can conclude that in annular flow smaller droplets which can follow the gas phase turbulence more closely have small slip velocity and increase of concentration of such droplets attenuate the turbulence intensity. On the other hand larger droplets move at relatively slow velocity and do not follow the turbulence very closely. Accordingly the increase of concentration of such droplets enhances the turbulence intensity.

As mentioned earlier, in annular flow, droplet size and velocity distribution is function of gas and liquid phase flow rates. For a given liquid flow rate as the gas velocity increases, the amount of entrained liquid also increases. Initially at low gas velocity, most of the liquid flow in the form liquid film and film thickness and disturbance wave amplitude are relatively large (see Sawant et al., 2008b). Since the disturbance waves are the major source of droplets in annular flow (Ishii and Grolmes, 1975; Kataoka et al. 1983), the droplet size distribution directly depends on the disturbance wave amplitude. Therefore, under low gas velocity condition, droplets are relatively large. As the gas velocity increases, more and more liquid gets entrained into the gas core and liquid film flow rate gradually decreases resulting in decrease of disturbance wave amplitude. Consequently the average size of droplets also decreases with the increase in gas velocity. Similar trends are shown by the droplet size correlations proposed by Kataoka et al. (1983) and Azzopardi et al. (1980). The predictions of these correlations for the air–water flow at 4.0 bar in 10 mm pipe are plotted in Fig. 11. It can be observed that the mean droplet size decreases to less than 40 μm for the gas velocity greater than 50 m/s. Additionally, as mentioned earlier, it is also expected that the smaller droplets under high gas velocity follow the gas phase turbulence more closely resulting in lower relative velocity and lower particle Reynolds number. Under the condition of maximum entrainment fraction, the liquid film is thin and amplitude of disturbance waves is very small (of the order of 50 μm or smaller; see Sawant et al., 2008b). A size of the droplets created from such waves is also very small. It is expected that under this high gas velocity condition, increase of droplet concentration with the increase in liquid flow rate may actually suppress the gas phase turbulence intensity. This may result in decrease of interaction between the gas flow and liquid film or the increase of effective thickness of gas phase viscous sublayer. Consequently the minimum liquid film flow rate at the maximum entrainment fraction increases with the increase of total liquid flow rate. Summarizing the above discussion we can conclude that the increase of Re_{ffmin} with the increase in Re_f is due to the effect of droplet concentration on gas phase turbulence.

Contrary to the above conclusion, Azzopardi (1997) and Hay et al. (1996) proposed the enhancement of turbulence with the increase in droplet concentration. However, they arrived at this conclusion based on the results of air–water experiment data obtained at relatively low gas velocities (30-36 m/s) compared to the gas velocities at the maximum entrainment fraction or minimum liquid film flow rate (Re_{ffmin}) condition. On the other hand, Namie and Ueda(1972) who proposed the suppression of turbulence with the increasing droplet concentration, performed their experiments at relative high gas velocities (43 to 58 m/s) where measured droplet diameter varied from 23 to 40 μm. Based on their measurement of droplet slip velocity and droplet diameter, the maximum particle Reynolds number calculated is always less 100. Further detailed

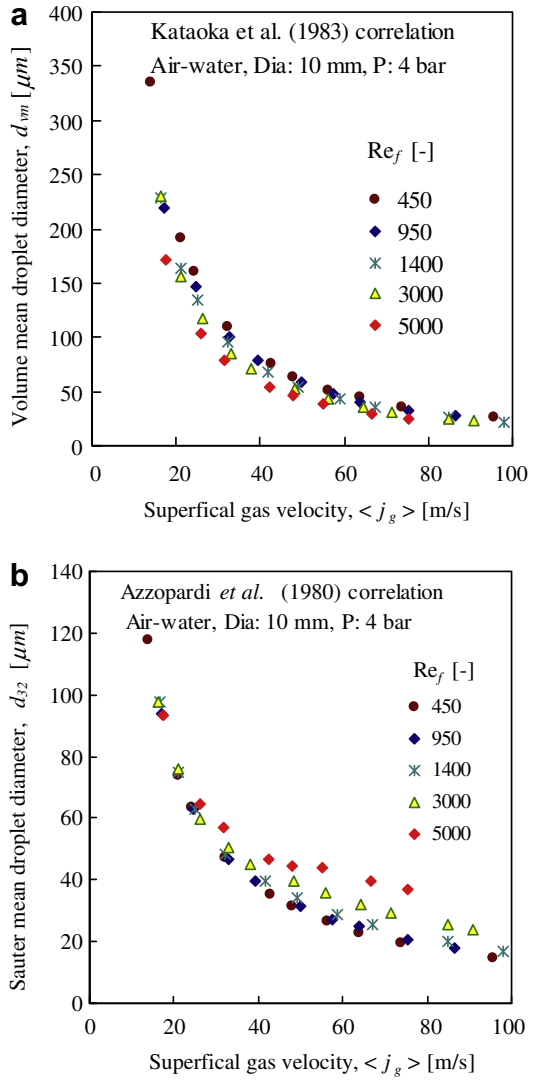

Fig. 11. Variation of mean droplet diameter: (a) Kataoka et al. (1983) correlation and (b) the Azzopardi (1980) correlation.

analysis and measurement of turbulence intensity under high gas velocity condition are necessary in order to substantiate the above conclusion. In this study, air–water data in Fig. 5 is used to obtain an empirical correlation to predict the effect of droplets on Re_{ffmin} as follows;

$$f(Re_{fEX}) = f(Re_f - Re_{ffOE}) = 0.3(Re_f - Re_{ffOE})^{0.95} \quad (20)$$

Substituting the above equation for $f(Re_{fEX})$ and Eq. (17) for Re_{ffOE} in Eq. (9), the following equation can be obtained for the prediction of Re_{ffmin};

$$Re_{ff\,min} = 13N_{\mu f}^{-0.5} + 0.3(Re_f - 13N_{\mu f}^{-0.5})^{0.95} \quad (21)$$

Fig. 5 shows the comparison of the above correlation with the experimental data. It can be observed the correlation satisfactorily predicted the air–water experimental data. However, it is derived based on air–water data and there is an uncertainty regarding its applicability under different fluid property conditions. The experimental data on measurement of Re_{ffmin} using different fluids is necessary to verify the above correlation. Since these experiments should be performed at very gas velocity condition, such experimental data is not available in literature. Instead, in Section 5, the applicability of the above correlation under different fluid property conditions is verified by comparing the entrainment fraction correlation Eq. (7) with Eq. (19) used to calculate E_{max} with the experimental data measured in Freon-113 experiments.

5. Evaluation of entrainment fraction correlation

The newly developed correlation for the prediction of entrainment fraction is compared with the air–water and Freon-113 experimental data obtained in the current study. Also the comparison of the correlation with Willetts's (1987) air–water, helium-water and air-genklene data and several other steam–water data is presented in this section. Table 3 shows a summary of the experimental data selected for the comparison with the correlation.

The following final form of entrainment fraction correlation can be obtained by combining Eqs. (7)–(19);

$$E = \left(1 - \frac{13N_{\mu f}^{-0.5} + 0.3(Re_f - 13N_{\mu f}^{-0.5})^{0.95}}{Re_f}\right) \times \tan h\left(2.31 \times 10^{-4} Re_f^{-0.35}(We - We_{cr})^{1.25}\right) \quad (22)$$

It can be observed that the correlation depends only on non-dimensional numbers Re_f, We, We_{cr} and $N_{\mu f}$. It is also simple and explicit and can be incorporated into the system analysis codes very easily. Critical Weber number, We_{cr} is calculated from Ishii and Grolmes criteria presented in Eqs. (10) and (11). The above correlation can be further simplified by neglecting the critical Weber number, We_{cr}. It was found that this assumption do not affect the overall prediction of the correlation. The following simplified correlation is compared with the experimental data listed in Table 3:

$$E = \left(1 - \frac{13N_{\mu f}^{-0.5} + 0.3(Re_f - 13N_{\mu f}^{-0.5})^{0.95}}{Re_f}\right) \tan h(2.31 \times 10^{-4} Re_f^{-0.35} We^{1.25}) \quad (23)$$

Table 3
Entrainment fraction experimental data

Data Source	Fluid system		P [bar]	σ [N/m]	μ_f/μ_g [–]	ρ_f/ρ_g [–]	$N_{\mu f}$ [–]×10^{-3}
Current Data	Air–water		1.2	0.072	55.56	768	2.26
	Air–water		4.0	0.072	55.56	208	2.26
	Air–water		6.0	0.072	55.56	143	2.26
	Freon-113		2.8	0.010	29.46	67	3.14
	Freon-113		5.0	0.008	23.36	40	3.03
	Freon-113		8.5	0.006	17.66	22	3.08
Willettes (1987)	Air–water		1.5	0.072	54.35	545	2.26
	Helium-water		1.5	0.072	54.35	3696	2.26
	Air-genklene		1.5	0.025	46.74	544	4.02
Steam–water data	Wurtz (1978)	Steam–water	69.0	0.017	4.76	20	0.64
	Singh et al. (1969)	Steam–water	69.0	0.017	4.76	20	0.64
	Keeys et al. (1970)	Steam–water	34.0 to 69.0	0.028 to 0.017	6.44 to 4.76	48 to 20	0.53 to 0.64
	Nigmatulin et al. (1976)	Steam–water	10.0 to 50.0	0.042 m to 0.022	8.75 to 5.56	173 to 31	0.71 to 0.58

5.1. Comparison with air–water and Freon-113 data

As shown in Table 3, the current air–water data covered three pressure conditions 1.2, 4.0 and 5.0 bar and five liquid flow rate conditions. At each liquid flow rate, the gas velocity is varied in such a way that entrainment fraction changes from very low to the maximum entrainment fraction (E_{max}) under high gas velocity. The table also shows the values of surface tension (σ), density ratio (ρ_f/ρ_g), viscosity ratio (μ_f/μ_g) and viscosity number ($N_{\mu f}$). It can be observed that the density ratio in air–water experiments varies from 143 to 768. Since the viscosity ratio and surface tension are constant, the viscosity number is also constant. Consequently the liquid phase Reynolds number at the onset of entrainment (Re_{ffOE}) calculated by Eq. (9) is 273 and constant for all the air–water data. Fig. 2 shows the comparison of the new correlation, Eq. (21) with the air–water data. It can be observed that the correlation satisfactorily predicted the trends in variation of entrainment fraction including the trends in maximum entrainment fraction observed under high gas velocity. In Fig. 12, the predicted entrainment fraction is plotted against the experimental entrainment fraction. Most of the experimental data is predicted within ± 20 % range.

The organic fluid experiments are performed using Freon-113 as a working fluid at three pressure conditions, 2.8, 5.0 and 8.5 bar. Fig. 4 shows the detailed liquid and gas flow rate conditions at each pressure plotted on flow pattern map. From Table 3, it can be observed that contrary to the air–water experiments, in Freon-113 experiments the density ratio, surface tension as well as viscosity ratio changes with pressure. The surface tension and density ratio are very low compared to the air–water experiments. Furthermore, it can be observed that all these parameters are close to the steam–water condition at 70 bar. Particularly the density ratio at 8.5 bar in Freon-113 is very similar to the density ratio at 70 bar in steam–water system. Therefore, it can be assumed that Freon-113 data can simulate high pressure steam–water flow conditions. Since the viscosity number do not change much with pressure as well as it is very close to the air–water flow experiments, Re_{ffOE} is also very close to the air–water flow value. Re_{ffOE} calculated by Eq. (9) for Freon-113 experiments is approximately 234.

In the following analysis of Freon-113 data, first the ability of Weber number to collapse the data at different pressure conditions is verified. Since the density ratio change is the most dominant change between the three pressure conditions it is expected that Weber number should collapse the data at different pressure conditions. The experimental data measured at liquid phase Reynolds number approximately 10000 and 14000 are plotted against the gas velocity in Figs. 13a and 13b, respectively. It can be observed that as the pressure increases for a given gas velocity the entrainment fraction increases. Also the entrainment fraction increases with the increase in gas velocity. Similar trends were observed in the air–water data analyzed in Sawant et al. (2008a). Figs. 13c and 13d shows the same data in Figs. 13a and 13b plotted against Weber number. It can be observed that Weber number successfully predicted the pressure effect. Thus same non-dimensional numbers, Re_f and *We* which collapsed the air–water data also predicted the effect of pressure in Freon-113 data. Now we will consider the comparison of the new correlation with Freon-113 experimental data. The predicted entrainment fraction is plotted against the experimental entrainment fraction in Fig. 14. Even though the higher entrainment fraction data is slightly over-predicted and some lower entrainment fraction data is under-predicted, in the overall most of the data is predicted within ± 20 % range.

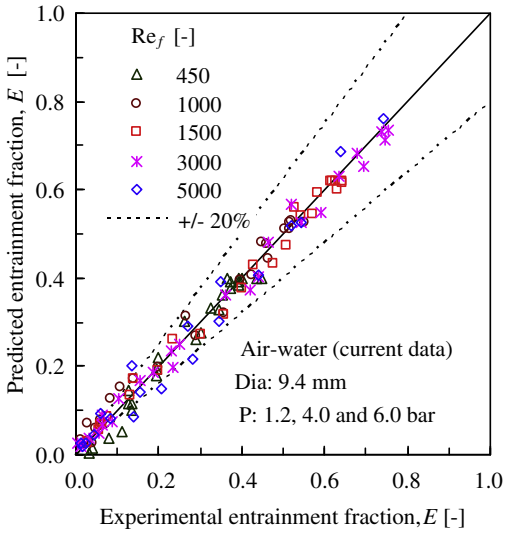

Fig. 12. Comparison of the new correlation Eq. (21) with current air–water data.

5.2. Comparison with Willetts's air–water, helium-water and air-genklene data

Willetts (1987) performed annular flow experiments near atmospheric pressure condition in 10.2 mm diameter test section using air–water, helium-water, air-sulpholane, air-genklene and air-fluoroheptane systems. In this study, the new correlation is compared with their air–water, helium-water and air-genklene data. The air-sulpholane and air-fluoroheptane data showed unusual trends (Pan and Hanratty, 2002) and not considered for the comparison with the correlation. As shown in Table 3, the helium-water data is corresponds to high density ratio condition while the viscosity ratio and surface tension are similar to air–water data. Air-genklene data is useful for studying the effect of surface tension. The surface tension of genklene is 0.025 N/m while other properties such as density ratio and viscosity ratio are very similar to air–water system at atmospheric pressure. Fig. 15 shows the predictions of Willetts's experimental data by the newly developed entrainment fraction correlation. It can be observed that most of the data is predicted within ± 20 % range except the air–water data which is slightly over-predicted.

5.3. Comparison with steam–water data

High pressure steam–water entrainment fraction data measured by Wurtz (1978), Singh et al. (1969), Keeys et al. (1970) and Nigmatulin et al. (1976) are selected for the comparison with the new correlation. As shown in Table 3, the surface tension and density ratio for the steam–water data are very close to Freon-113 data. However, the viscosity ratio for steam–water conditions is relatively small compared to the air–water, Freon-113, helium-water and air-genklene experiment conditions. Furthermore, the viscosity number for the steam–water system is also less than the other fluid systems. Consequently Re_{ffOE} calculated by Eq. (9) is higher for the steam–water experiments.

The comparison of Wurtz (1978), Singh et al. (1969), Keey et al. (1970) and Nigmatulin et al. (1976) experimental data with the new correlation is shown in Figs. 16a, 16b, 16c and 16d, respectively. Additionally, the figures also show the range of liquid phase Reynolds number covered in each experiment. It can be observed that most of the experiments were performed at very high liquid phase Reynolds number conditions. The new correlation highly under-predicted Nigmatulin *et al.* and Wurtz's data. The predictions of Singh *et al.* and Keeys's data also shows significant scatter. On the contrary, Freon-113 data having very similar fluid properties was predicted well by the correlation.

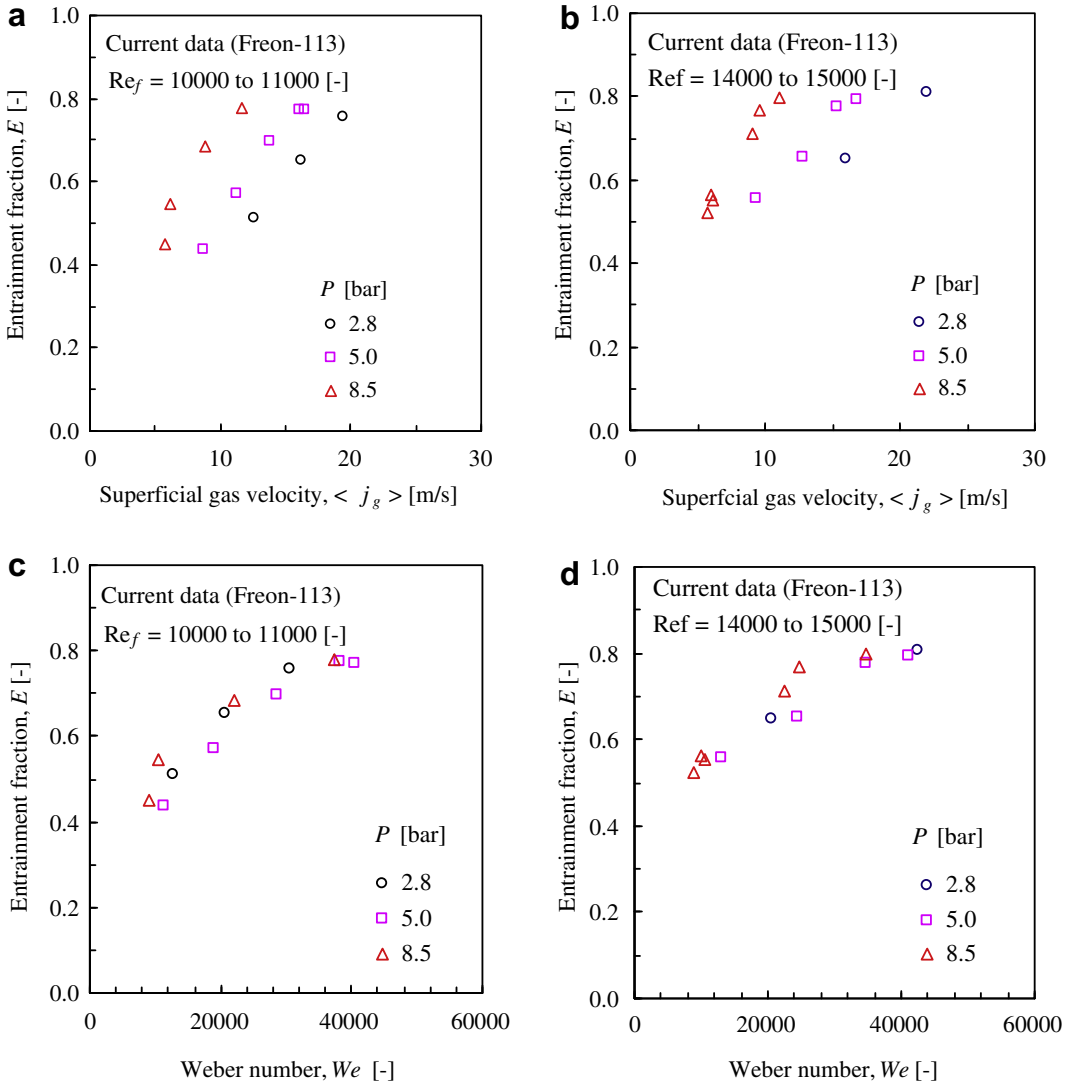

Fig. 13. Analysis of Freon-113 data.

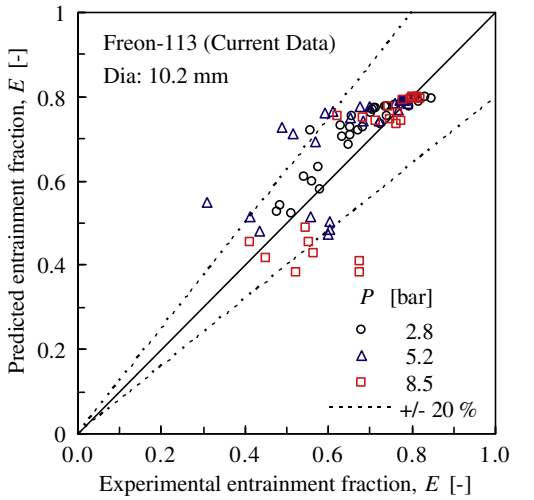

Fig. 14. Comparison of the new correlation Eq. (21) with current Freon-113 data.

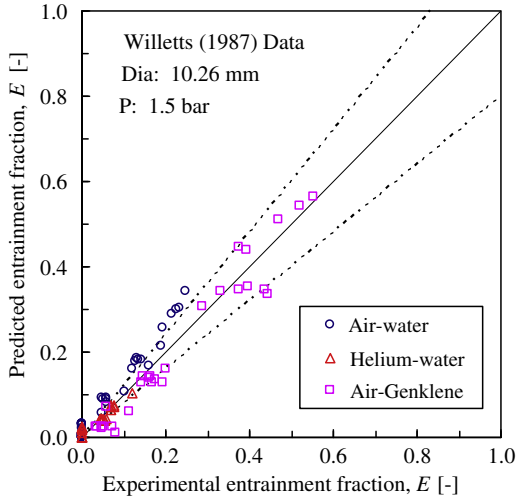

Fig. 15. Comparison of the new correlation Eq. (21) with Willettes data.

Two possible reasons have been identified for this discrepancy. The first is a measurement error associated with the limitations of measurement method and the second one is a change in mechanism of entrainment. All the steam–water experiments

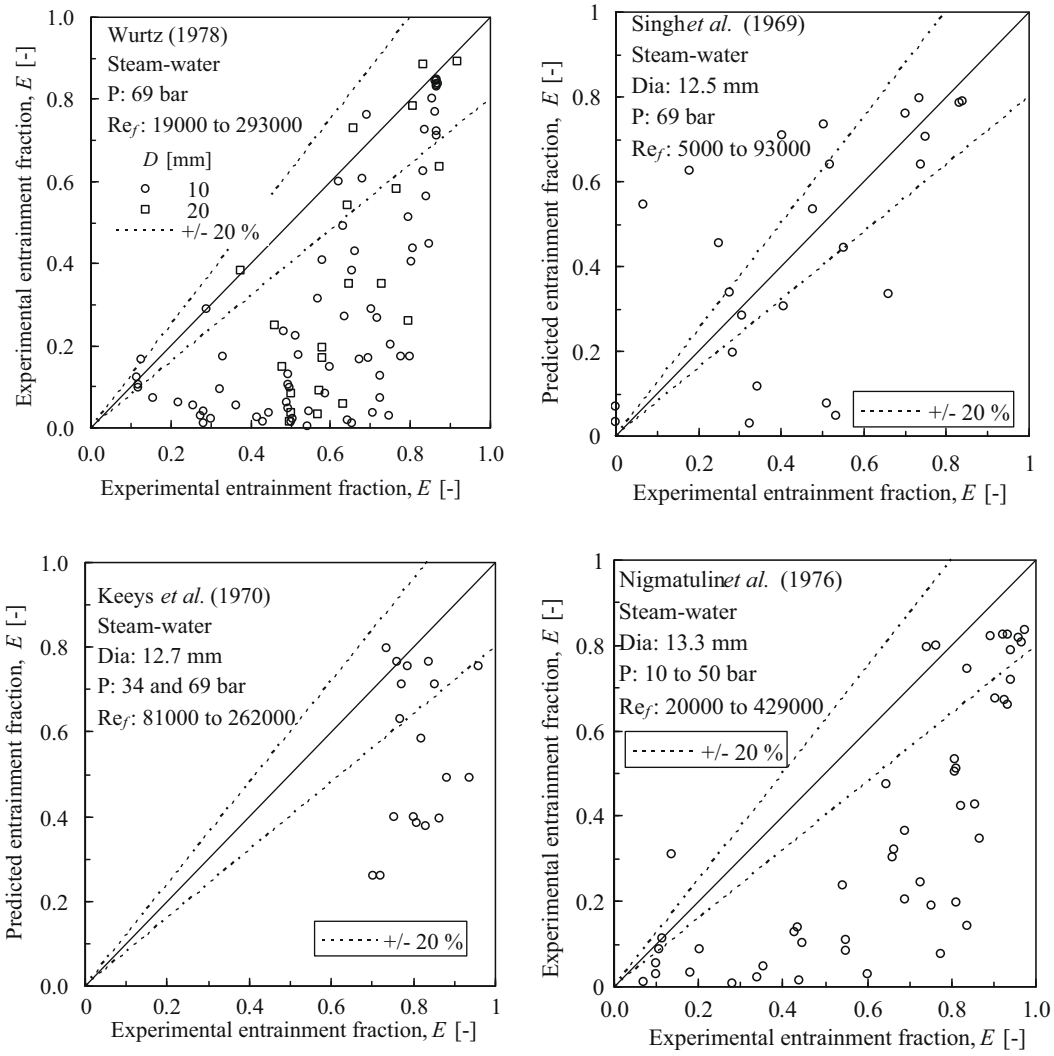

Fig. 16. Comparison of the new correlation Eq. (21) with the steam–water data: (a) Wurtz (1978) data, (b) Singh et al. (1969) data, (c) Keeys et al. (1970) data, (d) Nigmatulin et al. (1976) data.

employed the liquid film extraction method for the measurement of entrainment fraction. As discussed earlier in the introduction of this paper, this measurement method is constrained by the possibility of incomplete extraction of the liquid film. At higher liquid phase Reynolds number, the transition to annular wispy flow takes place. Based on the limited experimental data available in literature it was found that the liquid film in the transition region and in annular wispy flow region is covered by huge waves having high velocity compared to the regular disturbance waves observed in annular mist flow (Sekoguchi and Takeishi, 1989). Additionally, the liquid film is also very thick under high liquid phase Reynolds number conditions. The large waves may escape the extraction in film extraction unit resulting in overestimation of the entrainment fraction and hence the under-prediction of the experimental data by the correlation. Furthermore, in annular wispy flow, the mechanism of entrainment might be quite different than the entrainment due to the shearing off the crest of disturbance waves observed in annular mist flow. Other entrainment mechanisms such as liquid bridge break-up reported by Ishii and Grolmes (1975) may play important role in annular wispy flow. A further study on transition from annular mist to wispy flow and measurement of liquid film and entrainment fraction in this region is essential in order to understand and model the entrainment in annular wispy flow.

6. Conclusion

1. A new correlation is developed for the prediction of entrainment fraction as given below:

$$E = \left(1 - \frac{13N_{\mu f}^{-0.5} + 0.3(Re_f - 13N_{\mu f}^{-0.5})^{0.95}}{Re_f}\right) \times \tan h\left(2.31 \times 10^{-4} Re_f^{-0.35}(We - We_{cr})^{1.25}\right)$$

2. The correlation is simple, non-dimensional and explicit and accounts for the existence of critical gas and liquid velocities below which no entrainment is possible.
3. A new correlation is also proposed for the prediction of minimum liquid film Reynolds number (Re$_{ffmin}$, Eq. (19)) necessary for the estimation of maximum possible entrainment fraction for a given liquid flow rate. Furthermore, a correlation is developed for the predictions of liquid film Reynolds number at the onset of entrainment under high gas velocity (Re$_{ffOE}$, Eq. (17)) using the newly obtained air–water experimental data on onset of disturbance wave condition as well as the extensive data available in literature. It is also proposed that the dependence of Re$_{ffmin}$ on liquid phase flow rate is due to the suppression of gas phase turbulence intensity with the increase in droplet concentration.

4. The newly developed entrainment fraction correlation is satisfactorily compared with the air–water and Freon-113 experimental data collected in this study as well as the air–water, helium-water and air-genklene data of Willetts (1987) and several steam–water data available in literature. The probable reasons behind the failure of the correlation to predict the steam–water data are discussed.
5. The new entrainment fraction correlation is applicable for the test section diameters up to 32.0 mm. Above this diameter, disturbance waves become non-coherent and further study is necessary to model the entrainment phenomenon in large diameter pipe. The correlation is also limited to the annular mist flow conditions. A reliable data on the measurement of entrainment fraction and disturbance wave characteristics in the transition regime between annular mist and annular wispy flow and in the annular wispy flow regime are necessary for the further improvement of the entrainment fraction correlation.

Acknowledgements

The research project was supported by Tokyo Electrical Power Company (TEPCO). The authors would like to express their sincere appreciation for support from the TEPCO.

References

Abolfadl, M., Wallis, G.B., 1985. A mixing length model for annular two-phase flow. PCH PhysicoChemical Hydrodynamics 6 (1–2), 49–68.
Asali, J.C., 1984. Entrainment in vertical gas–liquid annular flows. Ph.D. Thesis, Department of Chemical Engineering, University of Illinois, Urbana, USA.
Azzopardi, B.J., Freeman, G, King, D.J., 1980. Drop sizes and deposition in annular two-phase flow. UKAEA Report AERE R9347.
Azzopardi, B.J., Taylor, S., Gibbons, D.B., 1983. Annular two-phase flow in large diameter pipes. In: International Conference on Physical Modelling of Multi-Phase Flow, pp. 267–282.
Azzopardi, B.J., 1997. Drops in annular two-phase flow. International Journal of Multiphase Flow 23 (suppl.), 1–53.
Azzopardi, B.J., 1999. Turbulence modification in annular gas–liquid flow. Int. J. Multiphase Flow 25 (6), 945–955.
Bennett, A.W., Hewitt, G.F., Kearsey, H.A., Keeys, R.K.F., Lacey, P.N.C., 1965. Flow visualization studies of boiling at high pressure. Proc. Inst. Mech. Eng. 180 (Part 3C), 1–11.
Gill, L.E., Hewitt, G.F., Lacey, P.M.C., 1964. Sampling probe studies of gas core in annular two-phase flow. Chem. Eng. Sci. 19 (9), 665–682.
Gore, R.A., Crowe, C.T., 1989. Effect of particle size on modulating turbulence intensity. Int. J. Multiphase Flow 15 (2), 279–285.
Hall-Taylor, N.S., Nedderman, R.M., 1968. The coalescence of disturbance wave in annular two-phase flow. Chem. Eng. Sci. 23 (6), 551–564.
Hawkes, N.J., Lawrence, C.J., Hewitt, G.F., 2000. Studies of annular-wispy flow using transient pressure gradient and optical measurements. Int. J. Multiphase Flow 26 (10), 1565–1582.
Hay, K.J., Liu, Z.C., Hanratty, T.J., 1996. Relation of deposition rates to drop size at large concentrations. Int. J. Multiphase Flow 22 (5), 829–848.
Hetsroni, G., 1989. Particles-turbulence interaction. Int. J. Multiphase Flow 15 (5), 735–746.
Hewitt, G.F., Roberts, D.N., 1969. Study of two-phase flow pattern by simultaneous X-ray and flash photography. UKAEA Report AERE-M2159.
Hills, J.H., 1997. The critical liquid flow rates for wave and droplet formation in annular gas–liquid flow. Exp. Heat Transfer Fluid Mech. Thermodyn. Ed. ETS 2, 1241–1247.
Ishii, M., Grolmes, M.A., 1975. Inception criteria for droplet entrainment in two-phase concurrent film flow. AIChE Journal 21 (2), 308–318.
Keeys, R.F.K., Ralph, J.C., Roberts, D.N., 1970. Liquid entrainment in adiabatic steam–water flow at 500 and 1000 psia. UKAEA Report AERE-R6293.
Kataoka, I., Ishii, M., Mishima, K., 1983. Generation and size distribution of droplet in annular two-phase flow. Journal of Fluids Engineering Transactions of the ASME 105 (2), 230–238.
Lopez de Bertodano, M.A., Assad, A., Beus, S.G., 2001. Experiments for entrainment rate of droplets in the annular regime. Int. J. Multiphase Flow 27 (4), 685–699.
Martin, C.J., 1983. Annular two-phase flow. D.Phil. Thesis, University of Oxford.
Martin, C.J., Azzopardi, B.J., 1985. Waves in vertical annular flow. PCH PhysicoChemical Hydrodynamics 6 (1–2), 257–265.
Mishima, K., Ishii, M., 1984. Flow regime transition criteria for upward two-phase flow in vertical tubes. Int. J. Heat Mass Transfer 27 (5), 723–737.
Namie, S., Ueda, T., 1972. Droplet transfer in two-phase annular mist flow, Part 1, experiment of droplet transfer rate and distributions of droplet concentration and velocity. Bulletin of the JSME 16 (90), 1568–1580.
Nedderman, R.M., Shearer, C.J., 1963. The motion and frequency of large disturbance waves in annular two-phase flow of air–water mixtures. Chem. Eng. Sci. 18 (10), 661–670.
Nigmatulin, B.I., Malyshenko, V.I., Shugaev, Y.Z., 1976. Investigation of liquid distribution between he core and the film in annular dispersed flow of steam/water mixture. Teploenergetika 23, 66–68.
Ohba, K., Nakamura, K., Naimi, F., 1995. A new kind of interfacial wave on liquid film in vertical upward air–water two-phase annular flow. In: Proceedings of the Second International Conference on Multiphase Flow, Kyoto, Japan.
Owen, D.G., Hewitt, G.F., 1987. An improved annular two-phase model. In: Proceedings of the Third International Conference on Multi-Phase Flow, The Hague, Netherland.
Pan, L., Hanratty, T.J., 2002. Correlation of entrainment in annular flow. Int. J. Multiphase Flow 28 (3), 363–384.
Sawant, P.H., Ishii, M., Mori, M., 2007. Prediction of entrainment fraction in vertical annular two-phase flow. In: Proc. of 12th Int. Topical Meeting on Nuclear Reactor Thermal Hydraulics (NURETH-12), Pennsylvania, USA.
Sawant, P.H., Ishii, M., Mori, M., 2008a. Droplet entrainment correlation in vertical upward co-current annular two-phase flow. Nucl. Eng. Des. 238 (6), 1342–1352.
Sawant, P.H., Ishii, M., Mori, M., 2008b. Properties of disturbance waves in vertical annular flow. Nucl. Eng. Des. 238 (12), 3528–3541.
Schadel, S.A., 1988. Atomization and deposition rates in vertical annular two-phase flow. PhD. Thesis, Department of Chemical Engineering, University of Illinois, Urbana, USA.
Sekoguchi, K., Takeishi, M., 1989. Interfacial structure in upward huge wave flow and annular flow regimes. Int. J. Multiphase Flow 15 (3), 295–305.
Shearer, C.J., Nedderman, R.M., 1965. Pressure gradient and liquid film thickness in co-current upwards flow of gas/liquid mixtures: application to film-cooler design. Chem. Eng. Sci. 20 (7), 671–683.
Singh, K., Pierre, C.C.St., Cargo, W.A., Moeck, E.O., 1969. Liquid film flow rates in two-phase flow of steam and water at 1000 psia. AIChE J. 15 (1), 51–56.
Willetts, I.P., 1987. Non-aqueous annular two-phase flow. D.Phil. Thesis, University of Oxford.
Wurtz, J., 1978. An experimental and theoretical investigation of annular steam water in tubes and annuli at 30 and 90 bar. Riso Report 372.